NIR FRET Luminescence in Rhenium Complex and Dye Co-Loaded Polymer Nanoparticles

Lucie Haye, Nour Fayad, Richard Knighton, Antoine Combes, Olivier Jeannin, Andrey Klymchenko, Thibault Gallavardin, Niko Hildebrandt, Loïc Charbonnière, Andreas Reisch

Near-Infrared FRET Luminescence in Rhenium Complex and Dye Co-Loaded Polymer Nanoparticles

Lucie Haye,[#a] Nour Fayad,[#b] Richard C. Knighton,[c] Antoine Combes,[a] Olivier Jeannin,[d] Andrey Klymchenko,[a] Thibault Gallavardin,[b] Niko Hildebrandt,*[b,e] Loïc J. Charbonnière,*[c] Andreas Reisch*[a]

Addresses

[a] Université de Strasbourg, CNRS, Laboratoire de Bioimagerie et Pathologies UMR 7021, Strasbourg F-67000 (France)

[b] Laboratoire COBRA (Chimie Organique, Bioorganique, Réactivité et Analyse), Université de Rouen Normandie, Normandie Université, CNRS, INSA Rouen, 76821 Mont Saint-Aignan (France).

[c] Equipe de Synthèse Pour l'Analyse (SynPA), Institut Pluridisciplinaire Hubert Curien (IPHC), UMR 7178, CNRS, Université de Strasbourg, ECPM, 25 rue Becquerel, 67087, Strasbourg Cedex (France)

[d] CNRS, ISCR-UMR 6226, Université de Rennes, F-35000 Rennes,F(rance)

[e] Department of Chemistry, Seoul National University, Seoul 08826 (South Korea).

# Contributed equally.

* e-mail: niko.hildebrandt@univ-rouen.fr; l.charbonn@unistra.fr; reisch@unistra.fr

Abstract

Photoactive transition-metal complexes are a class of luminophore combining high photostability and long luminescence lifetimes. However, reduced optical performance in aqueous solutions have limited their use in biological systems. Herein, we investigate the physicochemical and photophysical properties, and bioimaging compatibility of Re diimine complexes and near infrared (NIR) emitting Cy5 dyes coencapsulated in polymer nanoparticles (NPs) made of polymethacrylates and biodegradable polyesters. By varying the polymers, we obtained NPs with sizes ranging from 20 to 70 nm and encapsulating up to 40 wt% of Re complexes, i.e., close to 11,000 Re complexes per NP. The photoluminescence (PL) quantum yields of the Re complexes increased circa eightfold to ~50% upon encapsulation (*vs* 6-7% in non-degassed acetonitrile), which resulted in PL brightness of up to 10^8 M^{-1} cm^{-1} and PL lifetimes of the order of 3-4 µs. Coencapsulation of Cy5 resulted in very bright NIR emission upon Re complex excitation. Very close Re-to-Cy5 donor-acceptor distances down to ~2 nm or less and FRET efficiencies over 90% were confirmed by PL lifetime measurements. The Re-Cy5 NPs entered into mammalian cells for high contrast PL imaging in both the visible and the NIR. Our detailed characterization provided a better understanding of the photophysical properties of the transition-metal-dye FRET NPs and present a vital step toward the efficient design of a new classes of bright luminescent NP probes.

Introduction

Photoluminescence (PL) based imaging and sensing techniques have been major contributors to advances in biology and medicine by helping to unravel the underlying mechanisms of normal and pathological biological functions and their use in sensitive, fast, and affordable diagnosis.[1–3] Their success relies strongly on the performance of the used probes, notably in terms of photophysical properties like spectral characteristics, brightness, and PL lifetimes, but also in terms of how these can be exploited in biological environments.[4] From the large diversity of existing contrast agents, photoactive transition-metal complexes that include d^6 species Ru^{II},[5] Os^{II},[6] Ir^{III},[7] and Re^{I} [8,9] are known to be photostable and long-lifetime luminophores, which enable time-gated detection for suppression of short-lifetime background autofluorescence.[10–13] They exhibit large Stokes shifts, principally due to energy transfer between the ligand and the metal, facilitating separation of excitation and emission wavelengths and limiting PL self-quenching. These photophysical features make such transition-metal complexes interesting candidates for *in cellulo* imaging. However, most of the photophysical properties of these complexes are reported in organic solvents[10] because of their low solubility in aqueous media, which induces a non-controlled aggregation and a loss of PL.

A general and particularly facile approach to obtain luminescent probes is to encapsulate high amounts of individual emitters in non-fluorescent nanoparticles (NPs), such as silica NPs,[14,15] and, in particular, polymer NPs.[16–18] Encapsulation allows to efficiently separate the emitters from the PL-quenching environment. At the same time, the NP can be used to control size and interactions of the probe with the biological environment, allowing to decouple the photophysical properties from the surface properties and physical chemistry of the nanoprobe. Furthermore, the possibility to encapsulate a large number of emitters in a single NP leads to higher absorption cross sections, making it possible to achieve very high PL brightness.[19] This approach was particularly successful for the encapsulation of fluorescent organic dyes in polymer NPs and has led to fluorescent NPs with emission wavelengths spanning practically the whole visible spectrum and reaching also into the near infrared (NIR),[16–18] while achieving very high fluorescence brightness and excellent performance in complex biological systems,[20,21] paving the way to advanced biosensing and bioimaging applications.[22–25] Various other types of emitters, including lanthanide complexes[26,27] or metal nanoclusters[28] were also successfully encapsulated.

Interestingly, the very high local concentrations of the emitters within such NPs can alter the emission properties. Typically, these high concentrations lead to the risk of aggregation-caused quenching (ACQ) of the fluorophores, limiting their brightness, which can be mastered using

aggregation-induced emission (AIE) dyes, bulky side groups or bulky counterions.[17] On the other hand, the very small distances between emitters can lead to new photophysical behavior, like whole particle blinking due to very efficient and fast energy transfer between the dyes.[29,30]

Transition-metal complexes have been mainly encapsulated in inorganic structures such as crystals[31], zeolites[32,33] or silica nanoparticles[34] with the purpose of improving their catalytic performance. More particularly, ruthenium complexes have also proven to be good candidates for anticancer therapy when encapsulated in single-walled carbon nanotubes[35] but also in organic matrices such as liposomes,[36] micelles,[37] or polymeric NPs.[38–40] However, encapsulation of PL transition-metal complexes have rarely been explored.[41,42] Because little is known about the properties and the performance of NPs loaded with high amounts of luminescent transition-metal complexes, we decided to investigate these systematically. In particular, we were interested in achieving high levels of encapsulation of the complexes, while maintaining a good control over NP properties, in order to study the influence of loading on the PL properties of the complexes. As luminescent compounds, we selected two types of Re-based ^{3}MLCT emitters (**Figure 1A**, abbreviated Re(phen) and Re(bipy) here), based on their luminescence properties and available literature procedures for their synthesis. Indeed, [Re(diimine)$(CO)_3$L] emitters display impressive quantum yields (QYs) up to 41% under anaerobic conditions,[43] making them ideal candidates for exploration in this study.

Beyond the intrinsic Re emission in such NPs, the tunability of the NP's optical properties via energy transfer from Re to coencapsulated fluorescent dyes presents a very interesting approach from both a fundamental and application viewpoint. Here, we used a cyanine 5 (Cy5) derivative 1,1'-dioctadecyl-3,3,3',3'-tetramethylindodicarbocyanine (DiD) that was coencapsulated at different concentrations in the Re complex-loaded NPs. On the one hand, this allowed to shift the emission wavelength toward the NIR, which is advantageous for bioimaging applications by combining advantages of both types of emitters, *i.e.* long lifetimes and long emission wavelengths without metal toxicity.[44] On the other hand, studying energy transfer between the Re complexes and the Cy5 further allowed to understand the photophysics of such systems, but also the encapsulation and organization of the luminescent compounds inside the NPs. Based on these results, we then evaluated the suitability of the obtained probes for bioimaging applications.

Materials and Methods

Materials

Poly(D-L-lactide-co-glycolide) (PLGA, acid terminated, lactide:glycolide=50:50, Mw 24,000-38,000 g mol^{-1}, Ref.: 719870, Lot: BCBV0402), was purchased from Sigma-Aldrich. The EMA and HEMA based polymers and copolymers were synthetized through free radical polymerization as described in detail

in the ESI pages 17 to 21 based on previously used procedures.[45] Analysis of their composition using NMR and methylation of carboxylic acid groups, where adequate, showed a good agreement between aimed and actual polymer composition (ESI **Figures S14, S15, S16**). The Re complexes were synthesized through adaptation of known literature protocols: $[Re(CO)_5Cl]$ was reacted with an appropriate diimine (2,2'-bipyridine or 1,10-phenanthroline) to yield the neutral $[Re(diimine)(CO)_3Cl]$ intermediates,[46] which were converted to the cationic derivatives through halide abstraction, followed by anion metathesis with NaF6-TPB (sodium salt of tetrakis(3,5-bis(trifluoromethyl)phenyl)borate)[47] to give the $[Re(diimine)(CO)_3(MeCN)]$F6-TPB complexes Re(phen) and Re(bipy) (**Figure 1 and S1**, details of synthesis and characterization can be found in the ESI).[48] Cy5/F5-TPB, the salt of DiD (Cy5) with lithium tetrakis(pentafluorophenyl)borate ethyl etherate (AlfaAesar, 97%), was synthesized through ion exchange followed by purification through column chromatography by adapting previously published procedures.[21,29]

Dimethylformamide (DMF, analytical grade), dimethylsulfoxide (DMSO, analytical grade), methanol (MeOH, analytical grade), tetrahydrofuran (THF) and acetonitrile (analytical reagent ≥99.5%) were obtained from Carlo-Erba. Milli-Q water (Millipore) and phosphate buffer (20 mM, pH 7.4, from Na_2HPO_4, ≥99% and $NaH_2PO_4\,H_2O$, ≥98%, Sigma-Aldrich) were used for preparation of NPs.

Preparation of NPs

Stock solutions of polymers were prepared at a concentration of 10 g L^{-1} in acetonitrile. These solutions were diluted to 2 g L^{-1} in acetonitrile, with 10 to 40 wt% of Re(phen) or Re(bipy) (relative to the mass of the polymer) and 0 to 5 wt% of Cy5 (more precisely Cy5/F5-TPB). These solutions were quickly added to a 9-fold volume excess of MilliQ water or phosphate buffer (pH 7.4, 20 mM) under shaking (Thermomixer comfort, Eppendorf, 1050 rpm at 21°C), followed by further dilution to the desired concentration. The obtained NPs were used over several months without showing alteration of their properties.

Dynamic Light Scattering (DLS)

The size of the obtained NPs were measured on a Zetasizer Nano series ZSP (Malvern Instruments). Each sample was measured 10 times with a run length of 10 s each. Volume-averaged values, determined by the Zetasizer software based on Mie theory, were used. Mean values give the average over at least three independent preparations, error bars correspond to standard error of the mean.

Spectroscopic Properties

Absorption spectra of the complexes and the complex loaded NPs were recorded on a Cary 5000 Scan ultraviolet−visible spectrophotometer (Varian). Emission spectra of the rhenium complexes were recorded on a FLSP 920 fluorescence spectrometer (Edinburgh Instruments). Emission and excitation spectra of the NPs were recorded on a FS5 Spectrofluorometer (Edinburgh Instruments).

Excitation was performed at 275 nm for Re(phen) and 307 nm for Re(bipy) and the spectra were recorded between 400 and 800nm. Further details are given in the ESI.

Fluorescence Lifetime

Fluorescence lifetimes of Re complexes and NPs were measured with a NanoLed-303 from Horiba Jobin Yvon Fluorolog. The details of the experimental and fitting procedures are given in the ESI.

Cell Culture

HeLa cervical cancer cell line (ATCC-CCL-2 Lot N°57818419) was grown in Dulbecco's modified Eagle's medium (DMEM, Sigma-Aldrich, D6546), supplemented with 10% fetal bovine serum (FBS, Sigma-Aldrich, F0804), 1% antibiotics (Pen Strep, Sigma-Aldrich, P4333), and 2 mM L-glutamine (Sigma-Aldrich, G7513) at 37 °C and 5% CO_2. The cells were passaged with trypsin-EDTA 0.05%.

Cell incubation with NPs

Cells were seeded at $2x10^5$ cells/dish onto glass bottom petri dishes (CELLview Petri dishes 35 × 10 mm, Greiner Bio-One, 627860) and incubated at 37 °C and 5% CO_2 overnight. The next day, the cells were washed with HBSS (Thermo Fisher Scientific - HBSS, 10x, calcium, magnesium, no phenol red). The Re(phen)-Cy5 loaded NPs, Re(phen) loaded NPs and Cy5 loaded NPs were diluted with Opti-MEM to have final concentration of 10 µg/ml for Re(phen) NPs and Re(phen)-Cy5 NPs and at concentration of 4 µg/ml for Cy5 NPs and then were incubated for 3 hours at 37 °C and 5% CO_2. After incubation, the cells were washed 2 times with HBSS to rinse off any free conjugates and 1.5 mL of Opti-MEM (1×, Gibco, 11058-021) was added to the cell dish for immediate observation under the microscope at 37 °C.

Imaging

For the imaging of Re(phen) loaded NPs and Re(phen)-Cy5 loaded NPs, cells were transferred to a live cell chamber (Oko lab) onto the microscope and kept at 37 °C during the whole acquisition time. Images of the NPs were acquired using an Olympus IX83 inverted microscope and illuminated with an X-Cite Exacte illumination source (Excelitas Technologies) through a 320 nm excitation band-pass filter (FF01-320/40-25, Semrock Inc.) and 458 nm dichroic mirror (FF458-Di02-25x36, Semrock Inc.). The fluorescence signal was detected using a 60x objective (UPLSAPO, Olympus) and a 100x objective (UPLSAPO, Olympus), a 520 nm emission filter (FF02-520/28-25, Semrock Inc.) for the donor channel, and a 707 nm emission filter (BP-707/16-25, Delta) for the acceptor channel. For the control experiments of Cy5 loaded NPs, a 607 nm excitation band-pass filter (BP 607/8, Delta) and 660 nm dichroic mirror (FF660-Di02-25x36, Semrock Inc.) and a 676 nm emission filter (FF01-676/29-25, Semrock Inc.) were used. PL signals were recorded using an iXon Ultra 888 EMCCD camera (Andor) with an acquisition time of 500 ms for Re(phen) loaded NPs and 50 ms for Cy5 loaded NPs. Images of

cells were acquired with x500 EM gain for Re(phen) loaded NPs and x50 EM for Cy5 loaded NPs. Differential interference contrast (DIC) images were acquired with 10 ms acquisition time and x2 EM gain. An illumination power of 82 W was used with a 320 nm excitation bandpass filter and 10 W with a 607 nm excitation band pass filter. iXon camera and Olympus microscope were controlled by Micromanager software.

To eliminate the autofluorescence at 520±14 nm, the image obtained at that wavelength was adjusted by subtracting the average intensity of autofluorescence observed in cells without NPs using the same excitation parameters (320±20 nm excitation, 82 W illumination power, 500 ms acquisition time, and x500 EM gain). In addition, the threshold was adjusted in both channels to eliminate any background noise, this allows more accurate analysis of the PL signals observed in both donor and acceptor channels.

3D imaging and z-stacking

The NPs were imaged using an Olympus IX83 microscope and illuminated with an X-Cite Exacte illumination source using 82 W source power through a 320 nm excitation band-pass filter (FF01-320/40-25, Semrock Inc.) and emission was collected at 520 nm emission filter (FF02-520/28-25, Semrock Inc.) for the donor channel, and a 707 nm emission filter (BP-707/16-25 Delta.) for the acceptor channel after passing through 458 nm dichroic mirror (FF458-Di02-25x36, Semrock Inc.). The fluorescence signal was detected using a 100x objective (UPLSAPO, Olympus), and the z-stack images were obtained by a displacement of 0.5 µm per step. The images were acquired with x500 EM gain and 500 ms acquisition time. Micromanager software was used to control the iXon camera and Olympus microscope. The 3D reconstruction images and the z-stacking images were treated using ImageJ, by adjusting the threshold in both channels, and for the donor channel, the autofluorescence of cells was subtracted.

Time-gated (TG) plate reader spectroscopy

Re(phen) loaded NPs made from PEMA-COOH 1% at 40 wt% Re(phen) loading with different amounts of Cy5 (0, 0.1, 0.5, 1, 2, 5 wt%) and NPs made of PEMA-COOH 1% loaded with 5wt% of Cy5 only (no Re(phen)) were added to black 96-well microliter plates for a total volume of 140 µl in each well. TG-FRET measurements were performed on the multimode fluorescence plate reader SPARK (Tecan) with an excitation wavelength of 303 nm (bandwidth 5 nm) and emission spectra recording from 350 nm to 800 nm (bandwidth 5 nm) to measure both Re(phen) and Cy5 emission (gain: 100; integration time: 20 µs; lag time: from 0 to 20 µs). The Re(phen) and Cy5 peak intensities of the spectra were used to analyze the influence of the lag time on the donor and acceptor PL intensities.

Results and Discussion

Synthesis and characterization of Re complexes

Two types of Re-based ^{3}MLCT emitters of the general formula [Re(diimine)$(CO)_3$(MeCN)] with the diimine being either 2,2'-bipyridine or 1,10-phenanthroline (MeCN = acetonitrile) were selected in view of their luminescence properties in solution. In order to optimize their encapsulation in polymer NPs, the bulky hydrophobic counterion F6-TPB was introduced through ion-exchange to produce compounds of the general formula [Re(diimine)$(CO)_3$(MeCN)] F6-TPB (diimine = 1,10-phenanthroline or 2,2'-bipyridine, abbreviated Re(phen) and Re(bipy), respectively **Figure 1A, Figure S1**). Bulky hydrophobic counterions form highly apolar salts with cationic dyes and thus ensure effective encapsulation into the apolar matrix of polymer NPs with minimized dye leakage and ACQ.[21,49] In particular, highly fluorinated tetraphenyl borates like F5-TPB and F6-TPB have proven to be efficient for optimizing encapsulation, due to their big seize and distribution of negative charge on the surface of the anion,[50,51] which is why these were chosen here. All compounds were characterized by ^{1}H, ^{13}C, ^{11}B, and ^{19}F NMR, mass spectrometry, and elemental analysis (**Figure S2-S11**). For co-encapsulation, a NIR-emitting cyanine dye based on the hydrophobic Cy5 derivative DiD with a corresponding counterion F5-TPB (noted Cy5 or Cy5/F5-TPB in the following, **Figure 1A**) was prepared *via* a similar anion metathesis procedure, according to a previous literature protocol.[52,53]

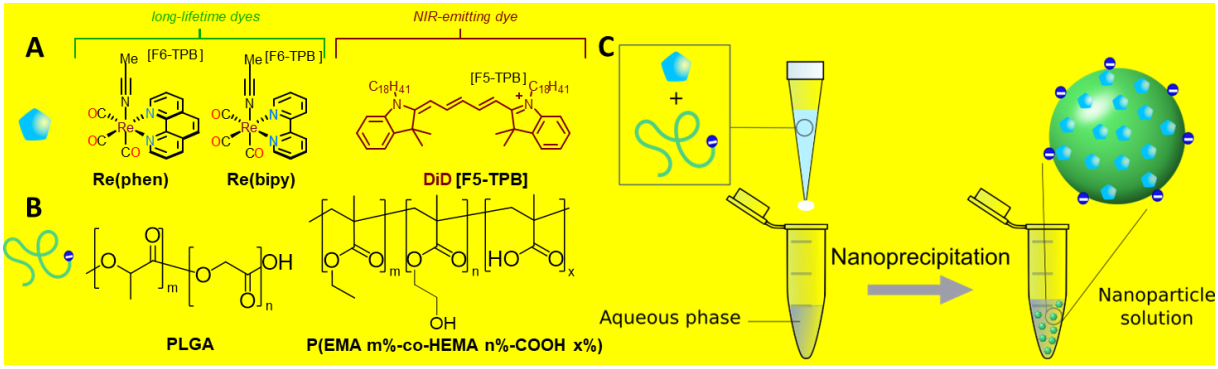

Figure 1 : A) Long-lifetime Re and NIR-emitting cyanine dyes used in this study ([F5-TPB] = tetrakis(pentafluorophenyl)borate, [F6-TPB] = tetrakis(3,5-bis(trifluoromethyl)phenyl)borate) B) Structures of polymers used for nanoparticles synthesis (PLGA = poly(lactic-co-glycolic acid) and P(EMA m%-co-HEMA n%-co-COOH x%)= Poly(ethyl methacrylate-co-hydroxyethyl methacrylate-co-methacrylic acid) with the following combinations: m = 99, n = 0, x = 1 ; m = 95, n = 0, x = 5 ; m = 75, n = 24, x = 1 ; m = 50, n = 49, x = 1. C) Scheme of the nanoprecipitation method used to synthesize NPs.

Single-crystals suitable for single crystal X-ray diffraction (SCXRD) were grown from slow evaporation of a concentrated CD_3CN solution of the Re(phen) complex (**Figure 2, Figure S12, S13**). The compound crystallizes in the P 2_1/n spacegroup (Z = 4) with one molecule in the asymmetric unit. The SCXRD structure confirmed the proposed formulation of the octahedral complex displaying a *fac*-arrangement of the carbon monoxide ligands with a single axially coordinated acetonitrile ligand. The

Re(phen) complex lay nested within a bis-aryl cleft formed by the F6-TPB anion. Bond lengths and angles were consistent with analogous complexes in the literature.[54,55]

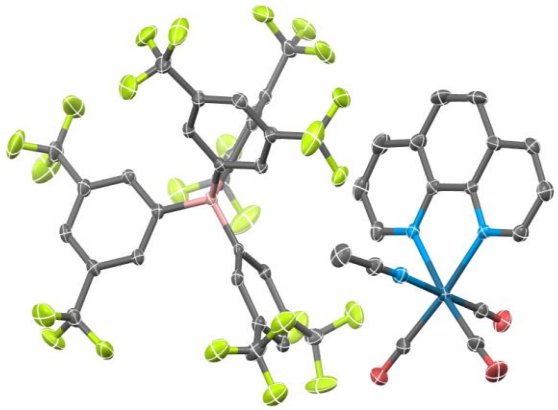

Figure 2. Single-crystal X-ray structure of the Re(phen) complex ([Re(1,10-phenenthroline)$(CO)_3$(MeCN)]F6-TPB) (ellipsoids plotted at the 50% probability level; H-atoms and disorder omitted for clarity) (CCDC: 2252609)

The spectroscopic properties of the molecular Re complexes were explored in aerated acetonitrile (**Table 1**). The absorption spectra for the free Re complexes showed two main features (**Figure S17**, **S18**), with ligand centered π-π* transitions dominating <320 nm, and broad visible maximum apparent at *ca*. 360 nm, corresponding to the ^{1}MLCT absorption band. The steady state photoluminescence spectra of both complexes gave broad structureless ^{3}MLCT emission at *ca*. 550 nm (**Figure S19**, **S20**). Time-resolved measurements revealed mono-exponential decays for the ^{3}MLCT of 150 ns and 247 ns for Re(bipy) and Re(phen), respectively (**Figure S21**, **S22**). QY measurements gave similar results for both complexes, 6-7% in aerated acetonitrile solutions.

Table 1. *Photophysical properties (absorption and emission maxima λ_{abs} and λ_{em}, PL lifetime τ, and PL QY Φ) of the obtained Re complexes in aerated acetonitrile at 298 K.*

	λ_{abs}/nm (ε /$M^{-1}.cm^{-1}$ × 10^5)	λ_{em}/nm	τ/ ns (% component)[a]	ϕ/ %[b]
Re(bipy)	268 (23,800), 306 (15,700), 317 (19,500), 350 (4,300)	558	150 (100%)	7
Re(phen)	273 (35,500), 366 (3,700)	548	247 (100%)	6

[a] Excitation at 452 nm using a NanoLed-303 from Horiba Jobin Yvon Fluorolog. [b] Using $[Ru(bipy)_3Cl_2]$ in water (Φ = 0.04; λ_{exc} = 450 nm) as a reference.[56]

Synthesis and characterization of NPs loaded with Re complexes

Nanoprecipitation was chosen for the synthesis of the complex-loaded polymer NPs (**Figure 1**), as it is a convenient and straightforward method to assemble NPs, which offers numerous possibilities to

tune composition and NP properties.[57,58] Particle formation in nanoprecipitation is a kinetically controlled process, occurring in a range of compositions of the solvent, water, polymer/load-system characterized by an initial high or very high supersaturation of polymer and load, in contrast to thermodynamically controlled assembly of polymer micelles. Here, the polymer and the complex to encapsulate were mixed in acetonitrile and the resulting mixture was added to an aqueous phase. While acetonitrile is totally miscible with water, both the polymers and the Re complexes were insoluble in water, leading to their assembly into NPs, trapping the complexes inside the polymer matrix. E.g. at these concentrations PEMA-COOH 5% precipitated already upon addition of ~10 vol% of water to the acetonitrile solution.[45]

In a first step, we optimized encapsulation of the Re complexes by varying their amount and the used polymer (**Figure 1B**). In particular, poly(ethyl methacrylate) (PEMA) based polymers bearing different amounts of charged methacrylic acid (MAA, noted COOH here) to tune the particle size were used. On the other hand, random copolymers of EMA with the hydrophilic hydroxyethyl methacrylate (HEMA), and poly(lactic-co-glycolic acid) (PLGA), a polymer known for its biocompatibility and biodegradability, were used to investigate the influence of polymer nature and hydrophobicity. Nanoprecipitation of both complexes, Re(phen) and Re(bipy), with the different polymers yielded NPs over the entire investigated range of loadings (10 to 40 wt% of Re complex relative to the polymer), with sizes ranging from 20 to 70 nm according to dynamic light scattering (DLS, shown in Erreur ! Source du renvoi introuvable.A for Re(phen)). The particle sizes decreased with increasing fractions of charged and hydrophilic groups on the polymers. The smallest NPs of about 20 nm were obtained with PEMA-COOH-5%, having the highest fraction of charged groups. PLGA yielded relatively small NPs of about 35 nm. Importantly, the amount of encapsulated complex led to no noticeable change in the size of the NPs for a given polymer. Together, this yielded a high tuning potential, as the size of the NPs could be finely controlled by modifying the structure of the polymer over a wide range of loadings. Both complexes yielded very similar results for the studied polymers and loadings, with Re(bipy) giving somewhat bigger particles with PLGA than Re(phen) (**Figure S39**). For selected examples, the sizes were also measured through transmission electron microscopy (TEM, **Figure S23**), yielding smaller sizes because TEM provides a number average of the hard-core diameter, but confirming the formation of spherical NPs with a monodisperse size distribution.

From the size determined by DLS, the number of complexes encapsulated per NP could be estimated using the size of the particle and the concentration of the Re complexes inside the NPs, going up to 11,000 Re complexes for the biggest NPs with the highest loadings (see ESI for details on the calculation and **Table S2** for results). These results allowed us to estimate the distances between Re complexes inside the NPs based on the Re complex concentration. Assuming that the Re complexes

were homogeneously distributed inside the NP, the mean center to center distance ranged from 2.8 nm for a loading of 10 wt% in Re complex to 1.9 nm for the highest loading, which suggested proximal Re complexes inside the NP.

This detailed characterization suggested that our nanoprecipitation approach allowed us to obtain Re complex-loaded polymer NPs (metallo-organic nano-hybrids) with excellent control over size and loading. However, it should be noted that nanoprecipitation of Re complexes alone, that was without the polymer, under identical conditions also yielded NPs in a similar size range. In consequence, the aforementioned results were insufficient to confirm the actual encapsulation of the Re complexes within the NPs, which will be addressed in more detail below in the sections on absorbance, PL, and FRET.

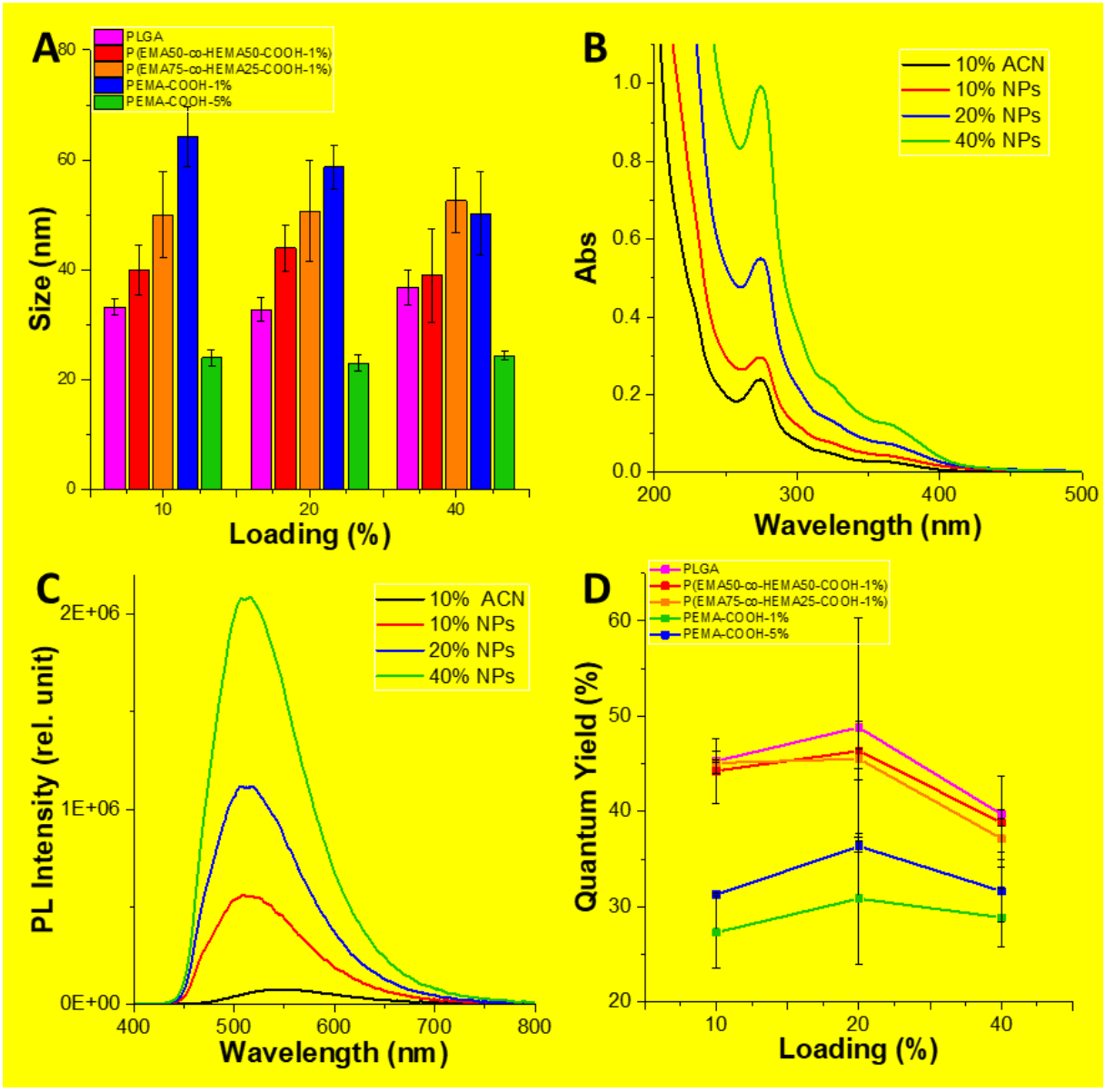

Figure 3 : A) Size for different NPs, B) absorbance, and C) emission (λ_{ex}=275 nm) spectra of Re(phen) in solution in acetonitrile or encapsulated in PEMA-COOH-1%. (Samples marked 10% ACN and 10% NPs have the same concentration in Re(phen). D) QYs for different NPs loaded with Re(phen), using Re(phen) in MeCN as a reference.

Absorption spectra of the Re complex loaded NPs (Erreur ! Source du renvoi introuvable.**B** for Re(phen), **Figure S40** for Re(bipy)) showed a peak around 275 nm for Re(phen) and at around 320 nm for Re(bipy), similar to those observed for the complexes alone in acetonitrile solution and characteristic of the ligand-centered transitions (*vide supra*). Noticeably, the difference between the absorbance spectra of the Re complex in ACN and in NPs at the same concentration was relatively low, this demonstrated that scattering was quite moderate by comparison with absorption. Together with the linear increase of absorbance with loading, this indicated a good encapsulation efficiency of the Re complexes inside the polymer matrix. Excitation of the Re(phen) and Re(bipy) loaded NPs at, respectively, 275 and 320 nm, resulted in both cases in a broad emission between 450 and 700 nm

(Erreur ! Source du renvoi introuvable.**C** and **Figure S41**). The PL intensity increased linearly with the loading, with maxima at around 510 nm for Re(phen) and 515 nm for Re(bipy) loaded NPs, somewhat blue shifted compared to the corresponding Re complexes in acetonitrile solution ($\lambda_{max} \approx 550$ nm). Interestingly, the emission intensity increased more than fivefold, when encapsulating the Re complexes in polymer NPs, compared to their simple dissolution in acetonitrile (for corresponding concentrations). For further characterization, we then focused on Re(phen) loaded polymer NPs, which exhibited a higher PL intensity than Re(bipy) when encapsulated in NPs. QY measurements in the case of the Re(phen) loaded NPs revealed that Re(phen) showed QYs up to 8-fold higher when encapsulated inside NPs (QY between 25 and 50%, Erreur ! Source du renvoi introuvable.**D**) compared to when dissolved in organic solvent (QY = 6%, **Table 1**). One might anticipate that energy transfer from the 3MLCT state of Re to triplet oxygen, which is one of the major quenching pathway of the luminescence,[59] is severely reduced by a decreased diffusion of oxygen in the solid NPs, as can be hypothesized based on observations on the effects of the matrix on Re(I)[60] and Cr(III)[61] emitters. Here, the observed increase in emission lifetimes (*vide infra*) effectively points towards decreased quenching upon encapsulation in the polymer nanoparticles, though the precise contribution of oxygen was not studied in detail. Considering the measured QYs, two groups of Re(phen) loaded NPs appeared depending on the used polymers: the NPs made with the more hydrophilic polymers (PLGA and EMA/HEMA copolymers) had higher QYs than the more hydrophobic PEMA based ones. We could also see that the extent of loading had little, or at least no clear, influence on the QY, suggesting that ACQ was not very important for these complexes. This is in line with the very large Stokes shift of these complexes, which limits homo-energy transfer and self-quenching. The brightness per NP was estimated based on the number of encapsulated Re complexes per NP, the QY, and the extinction coefficient of the Re complexes (see **Table 1**). The brightness increased with the loading and the particle size and a maximum brightness of 1.4×10^8 L mol^{-1} cm^{-1} was achieved for P(EMA 50 –HEMA 50-COOH-1% NPs (**Table S2**). These observations suggested that the encapsulation of the Re complexes inside polymeric NPs was a good way to enhance its emission and offered the possibility to create very bright Re PL.

Co-encapsulation of Re complexes and cyanine dyes

Re complexes emit in a spectral region with strong autofluorescence in biological environments, inducing high background signals. Hence, we aimed at shifting the emission wavelength towards the NIR, which would significantly reduce autofluorescence background.[44] NIR-emitting cyanine dyes are a typical example of fluorescent probes for autofluorescence-free and/or deep-tissue imaging.[62] In the case of transition-metal complexes, tuning the emission can be achieved by varying the energy landscape, which requires to profoundly change the chemical structure of the ligands.[63–66] An

alternative approach is the use of Förster resonance energy transfer (FRET) to NIR dyes, which can also induce a bathochromic shift in the emission of the luminescent system. This possibility was shown for a Ru-cyanine dyad, consisting of a Ru complex covalently linked to a Cyanine 5 dye.[67] The dyad could be used to induce long-lifetime downshifted PL, in which emission of Cyanine 5 (λ_{em}= 660 nm) was induced through excitation of the Ru ^{1}MLCT absorption band (λ_{ex} = 450 nm), which was operated *via* a FRET mechanism. Here, we used a similar FRET approach to shift the emission of the Re complexes into the NIR *via* a simple coencapsulation of cyanine dye FRET acceptors. We selected the Cyanine 5 based DiD as FRET acceptor and combined it with the bulky hydrophobic F5-TPB as counterion, noted Cy5/F5-TPB or simply Cy5 in the following (**Figure 1**), to improve encapsulation and avoid ACQ.[52]

Coencapsulation of 40 wt% of the Re(phen) complex with increasing amounts of Cy5 from 0.1, 0.5, 1, 2, to 5 wt% in PEMA-COOH 1% yielded NPs with only slight influence of the dye on the particle size as shown by TEM imaging (**Figure S23**, DLS not possible due to Cy5). Absorption spectra of the obtained NPs (**Figure 4A**) showed a linear increase of the absorbance of Cy5 with loading and constant Re(phen) absorbance, suggesting a good encapsulation of both chromophores. Furthermore, no significant changes in the shape of the absorption spectra was observed, indicating that the Cy5 dyes did not undergo extensive aggregation inside the NPs. The emission spectra showed a continuous decrease in the Re(phen) complex PL intensity with increasing Cy5 loading (**Figure 4B**). At the same time, Cy5 emission appeared even at the lowest Cy5 loading, and increased up to 2 wt% Cy5 loading. The decrease in emission intensity when going from 2 to 5 wt% loading suggest the appearance of ACQ effects at higher loadings. (It is interesting to note that the presence of the Re complex did not have a significant influence on the absorption spectra of the Cy5 encapsulated in the NPs, but a significant increase in the Cy5 emission in the presence of the complexes was observed, ESI Figure S30.)

Considering the PL intensities in the presence and in the absence of the acceptor (Cy5), the FRET efficiencies of these systems (**Table 2**) could be calculated according to Equation 22 (ESI). Globally, the FRET efficiency increased continuously with the amount of acceptor dyes going from 10 to 90 %. In this context it is noteworthy that the Re(phen) donor PL was only slightly quenched when adding 0.1% of Cy5 acceptor, whereas the acceptor PL increased significantly (direct excitation of Cy5 at the excitation wavelength of 292 nm resulted in only very low Cy5 PL – cf. **Figure S29, Table S3**), which means that the overall PL brightness of the Re(phen)-Cy5 NP system was improved via Re(phen)-to-Cy5 FRET.

The energy-level diagram depicted in **Figure 4C** gives a schematic view of the assumed downshifting behavior of the system co-encapsulating Re(phen) and Cy5. In the absence of Cy5 the Re(phen)

^{3}MLCT emission can be engendered *via* excitation of the ligand-centered S_1 ($\pi^*\leftarrow\pi$) or ^{1}MLCT absorption bands. Consequently, in the co-encapsulation particles containing Re and cyanine – and considered the very efficient FRET behavior – either of the Re(phen)-based absorption bands give rise to a populated ^{3}MLCT state which thus sensitizes the S_1 absorption band of the Cy5 dye at 642 nm with resultant Cy5 emission at 663 nm.

Table 2. FRET efficiencies for NPs loaded with 40 wt% Re(phen) and increasing amounts of Cy5, according to PL intensities.

Cy 5 loading (wt%)	*Number of Cy5 dyes per NP[a]*	*Average distance between Cy5 molecules (nm)[b]*	*Number of Re(phen) per Cy5[c]*	*FRET efficiency (%)*
0.1	*32*	*12.7*	*287*	*8*
0.5	*160*	*7.4*	*58*	*42*
1	*319*	*5.9*	*29*	*60*
2	*632*	*4.7*	*15*	*79*
5	*1534*	*3.5*	*6*	*92*

a) Calculated for 50 nm NPs as described in ESI. b) calculated according to ESI. c) for a Re(phen) loading of 40 wt%.

Energy transfer also offered the possibility to further study the actual encapsulation of the Re complexes inside the polymer NPs. For this, we encapsulated Re(phen) into NPs made with a polymer previously covalently grafted with Cy5. In this case, FRET can only occur for Re(phen) encapsulated within the polymer NPs, and not for NPs formed from the Re(phen) complexes alone. Excitation of the Re(phen) complex gave us a PL spectrum (**Figure S25 and S26**) corresponding to a Cy5 emission, accompanied by a strong decrease of the donor Re(phen) emission compared to NPs loaded with just Re(phen). The obtained decrease of Re(phen) emission was of the same order as for coencapsulation of Re(phen) and Cy5/F5-TPB at equivalent concentrations, indicating a very close proximity of Re(phen) and Cy5 attached to the polymer. In consequence, this result together with the arguments presented earlier, namely control of size through polymer and linear absorbance and PL of Re loaded NPs, supports the conclusion that the rhenium complexes are fully encapsulated inside the polymer NPs, with a very good encapsulation efficiency.

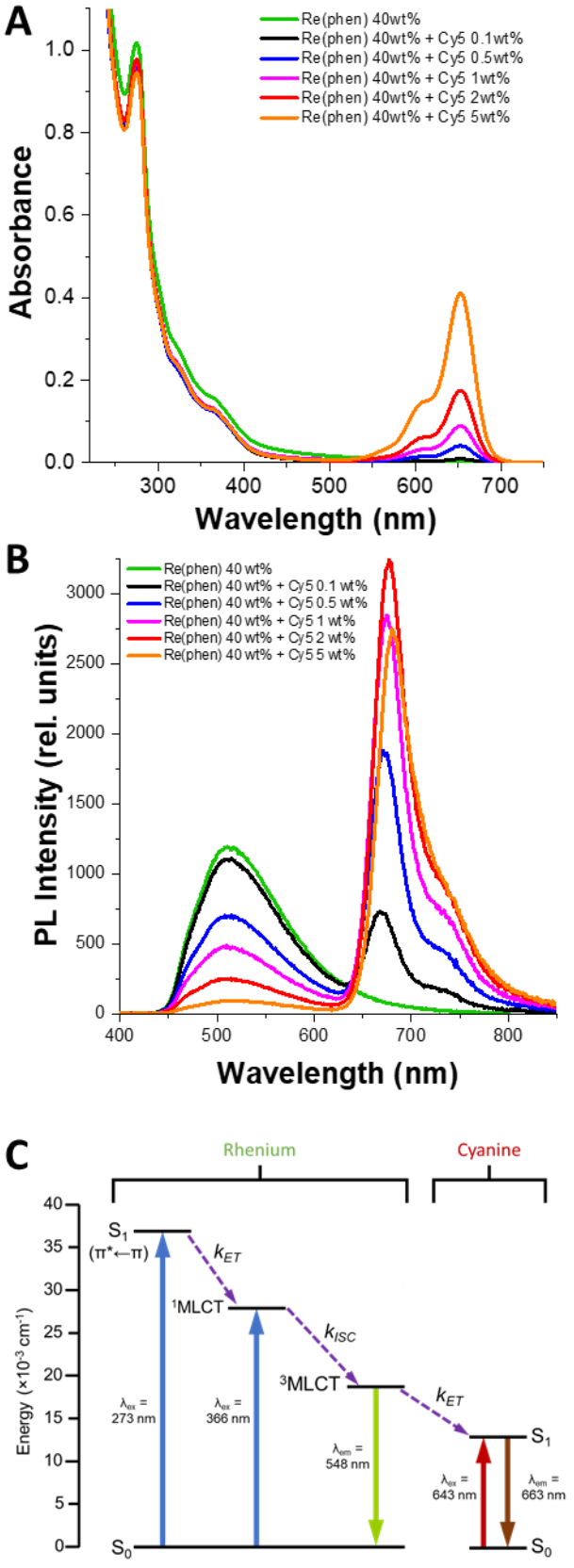

Figure 4 : A) Absorption spectra of NPs loaded with 40 wt% of Re(phen) and increasing amounts of Cy5. B) PL spectra of the same NPs excited at λ_{ex} =292 nm C) Energy level diagram for downshifting energy transfer processes within Re(phen) and Cy5 loaded NPs.

PL Lifetime Analysis

In order to better understand the photophysics of NPs loaded with Re complexes alone or coencapsulating Re complexes and Cy5, we decided to further investigate these systems *via* time-resolved PL spectroscopy. In particular, we wanted to study very high local concentrations of Re(phen) complexes and FRET between Re(phen) complexes and Cy5 dyes. Understanding the optical tunability of such hybrid systems is essential for an efficient implementation into biosensing and bioimaging applications.

In a first step, we studied the influence of encapsulation of Re(phen) complexes inside polymer NPs on their PL lifetimes. Compared to Re(phen) in solution (250 ns) the average PL lifetime strongly increased to over 3 µs inside the polymer NPs (**Table 3**), which provided good evidence for strongly reduced PL quenching when the Re(phen) complexes are protected from the environment by the polymer matrix. The double-exponential PL decay of Re(phen) in the NPs showed a shorter (~1.0 µs) and a longer (~4.6 µs) component, most probably related to Re(phen) complexes closer to the NP surface (prone to quenching *via* the environment) and closer to the NP center (better protection from the outer environment). Increased Re(phen) loading (from 10% to 20% and 40%) resulted in an overall better protection of the complexes from quenching by the environment, as shown by an amplitude increase (respectively decrease) of the longer (respectively shorter) component and thus, increasing amplitude-averaged PL lifetimes (3.1, 3.4, and 3.6 µs, respectively).

To study the influence of the presence of Cy5 acceptors, we measured the PL decays of both Re(phen) and Cy5 (**Figure 5**). With the intrinsic PL lifetime of Cy5 (few ns) being around 1000-fold shorter compared to the Re(phen) PL lifetime (~3.6 µs), the FRET-quenched Re(phen) PL lifetimes should in principle be visible in both Re(phen) and Cy5 emission. However, quite significant differences were found in the Re(phen) donor (**Figure 5A**) and Cy5 acceptor (**Figure 5B**) PL decays. The Re(phen) PL decays were relatively long, with amplitude-averaged PL decay times ranging from 3.26 µs (Re(phen) with 0.1% Cy5) to 0.67 µs (Re(phen) with 5% Cy5), which corresponded to system-averaged FRET efficiencies ($<E^*_{FRET}>$, which takes into account quenched and unquenched components) of ~10% and ~80% (**Table 3**). The Cy5 PL decays were significantly shorter, with amplitude-averaged PL decay times ranging from 0.69 µs (Re(phen) with 0.1% Cy5) to 0.06 µs (Re(phen) with 5% Cy5), which corresponded to $<E^*_{FRET}>$ values of ~80% and ~98% (**Table 4,** ESI for details on calculations). In addition, the PL intensities of the Cy5 dyes on the very short time scale (below ~200 ns in **Figure 5B**) were extremely high compared to those on the longer time scale (>500 ns). This very different decay behavior of FRET-quenched Re(phen) and FRET-sensitized Cy5 strongly suggested that there were many Re(phen) donors that did not interact with Cy5 acceptors and thus, $<E^*_{FRET}>$ values were much lower when measured via Re(phen) PL. A high fraction of unquenched

Re(phen) makes sense, in particular when the acceptor doping was very low, because in this case, the number of Re(phen) donors per Cy5 inside the NPs is very high (**Table 2**). Therefore, the FRET efficiencies calculated by donor PL intensity (**Table 2**) represent the system-averaged FRET efficiencies ($<E^*_{FRET}>$), which include both quenched and non-quenched Re(phen) donors and do not provide any donor-acceptor distance information (e.g., 50% non-quenched donors plus 50% donors with 100% FRET efficiency result in the same system-averaged FRET efficiency as 100% donors with 50% FRET efficiency). Hence, the actual FRET efficiencies (which only include donors that transfer energy to an acceptor) are most probably much higher than shown in the Re(phen) PL decays and the steady-state PL spectra. This assumption would also explain why the Cy5 acceptor sensitization is substantially stronger than the Re(phen) donor quenching (**Figure 4C**). Very efficient Re(phen)-to-Cy5 FRET becomes the preferred energy pathway compared to Re(phen)-Re(phen) homo FRET (which leads to self-quenching due to the increasing probability of ending up in a dark state with an increasing number of homo-FRET steps)[68] or Re(phen) PL quenching *via* the environment. This FRET configuration with reduced PL losses results in an overall emission amplification of the donor-acceptor system compared to the NPs loaded with Re(phen) alone. Thus, the PL QY of Re(phen) is not the same for Re(phen) loaded NPs and Re(phen)-Cy5 loaded NPs and the Re(phen) loaded NP PL spectrum cannot be used as correct donor-only FRET reference.

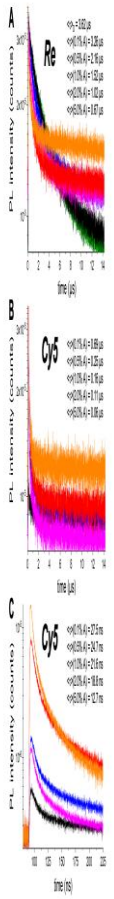

Figure 5: Excitation intensity-normalized PL decays ~~(intensities in each graph were normalized by the number of excitation pulses)~~ and amplitude-averaged lifetimes of Re(phen) loaded NPs containing distinct fractions of Cy5 (green: 0%; black: 0.1%; blue: 0.5%; magenta: 1%; red: 2%; orange: 5%) measured for Re(phen) donor (A: 515±8 nm) and Cy5 acceptor (B and C: 700±8 nm, ~~observation window 14 µs and 200 ns, respectively,~~) emission. Excitation via a 303±10 nm light emitting diode (pulse length < 1.2 ns). Note: To display PL decay curves with similar excitation conditions, the PL intensities in each graph were normalized by (i.e., divided by) the number of excitation pulses. This normalization resulted in a relatively strong intensity offset (constant background) at longer times for the higher Cy5 fractions (e.g., orange and red decay curves in A and B). The non-normalized decay curves are shown in Supporting Figures S31, S32, and S33 for A, B, and C, respectively.

PL decays could, in principle, be distinguished between quenched and unquenched components. If the non-quenched Re(phen) component can be identified in the decay curves, it is possible to extract it from the FRET components and an actual FRET efficiency, which considers FRET-pairs only, can be calculated. However, this can be quite challenging when the donor alone already possesses a multi-exponential decay (due to environmental quenching), which was the case of our Re(phen) complex-loaded NPs. We therefore used an approach that we previously applied to FRET from lanthanide complexes with multiexponential decays (see Equations 8 to 13 in ESI).[69,70] The Re(phen) loaded NP PL decay (green curve in **Figure 5A**) was fit with a bi-exponential function, which resulted in decay times of τ_{D0} = 4.51 µs, τ_{D1} = 1.14 µs, and $\langle\tau\rangle$ = 3.61 µs (amplitude-averaged decay time). The Cy5-containing NPs (black, blue, magenta, red, and orange curves in **Figure 5A**) were fit with a 3-

exponential function, for which the long decay time of Re(phen) (τ_{D0} = 4.51 µs) was fixed to account for the contribution of non-quenched Re(phen). The short decay component of Re(phen) (τ_{D1} = 1.14 µs) could not be extracted from the FRET decays by fixing because it had the same time range as the FRET decays. Therefore, an amplitude correction factor (z_D, Equation 11 in the ESI)[69,70] was used to correct for this contribution of free Re(phen) emission. By applying this method, two FRET decay times (τ_{DA1} and τ_{DA2}), their relative amplitudes (α_{DA1} and α_{DA2}), a relative donor amplitude (α_{DA0}), the donor correction factor (z_D), an average FRET decay time ($<\tau_{DA}>$), an average FRET efficiency ($<E_{FRET}>$), an average decay time of the complete decay ($<\tau>$), and a system-averaged FRET efficiency ($<E^*_{FRET}>$, taking into account quenched and unquenched components) could be determined (**Table 3**).

Whereas the overall amplitude-averaged decay time ($<\tau>$) resulted in FRET efficiencies ($<E^*_{FRET}>$) that corresponded quite well to the ones determined by steady-state intensities (because also the PL decay contains all donor components – *vide supra*), the FRET decay times ($<\tau_{DA}>$) and FRET efficiencies of the actual FRET pairs ($<E_{FRET}>$) were significantly larger, in particular for the NPs containing few Cy5 (0.1, 0.5, and 1 wt%), which showed strong contributions of Re(phen)-only PL (61, 34, and 20% relative donor amplitude). For the NPs with higher amounts of Cy5 (2 and 5 wt%), the differences were not that strong because of the significantly lower contributions of non-quenched Re(phen) (13 and 10% relative donor amplitude) to the PL.

*Table 3 : Fit (from Re(phen) PL decay curves in Figure 5Erreur ! Source du renvoi introuvable.**A**) lifetimes (τ) and amplitude fractions (α) and calculated correction factors (z_D), amplitude averaged FRET lifetimes ($<\tau_{DA}>$), average FRET efficiencies ($<E_{FRET}>$), overall amplitude-averaged lifetimes ($<\tau>$), lifetime system-averaged FRET efficiencies ($<E^*_{FRET}>$), and intensity system-averaged FRET efficiencies (int.$<E^*_{FRET}>$).*

Re(phen)	τ_{D1} (µs)	α_{D1}	τ_{D0}	α_{D0}	rel. errors	$<\tau_D>$ (µs)
10 wt%	0.88	0.43	4.69	0.57	3%	3.07±0.18
20 wt%	0.96	0.33	4.64	0.67	3%	3.42±0.21
40 wt%	1.14	0.27	4.51	0.73	3%	3.61±0.22

Cy5	τ_{DA1} (µs)	α_{DA1}	τ_{DA2} (µs)	α_{DA2}	α_{DA0}	rel. errors
0.1%	0.64	0.28	1.52	0.72	0.61	18%
0.5%	0.34	0.31	1.27	0.69	0.34	10%
1.0%	0.24	0.40	1.14	0.60	0.20	6%
2.0%	0.11	0.37	0.74	0.63	0.13	4%

5.0%	0.05	0.50	0.43	0.50	0.10	3%

Cy5	z_D	$<\tau_{DA}>$ (µs)	$<E_{FRET}>$	$<\tau>$ (µs)	$<E^*_{FRET}>$	int. $<E^*_{FRET}>$
0.1%	0.22±0.12	1.31±0.74	0.64±0.40	3.26±1.17	0.10±0.04	0.08±0.02
0.5%	0.12±0.04	0.95±0.27	0.74±0.25	2.16±0.43	0.40±0.10	0.41±0.08
1.0%	0.072±0.013	0.76±0.12	0.79±0.17	1.52±0.18	0.58±0.10	0.60±0.12
2.0%	0.047±0.006	0.47±0.05	0.87±0.15	1.02±0.08	0.72±0.10	0.80±0.16
5.0%	0.037±0.003	0.20±0.02	0.94±0.15	0.67±0.04	0.81±0.10	0.92±0.18

Relative errors provided in the table are related to τ and α and were estimated. Errors for z_D, $<\tau_{DA}>$, $<E_{FRET}>$, $<\tau>$, $<E^*_{FRET}>$, and int.$<E^*_{FRET}>$ (intensity calculated system-averaged FRET efficiency with intensity errors estimated as 10%) were calculated using error propagation.

Although the decay time fitting showed that the FRET efficiencies of the actual Re(phen)-Cy5 FRET pairs were much higher than determined from steady-state PL intensities or overall averaged PL lifetimes, strong contributions of non-quenched Re(phen) emission inevitably led to large errors, which were even larger (due to error propagation) when calculating FRET efficiencies (see, *e.g.* FRET efficiencies for Re(phen) loaded NPs with 0.1% Cy5 in **Table 3**). Because the FRET-sensitized Cy5 emission (700±8 nm) contained almost no background from non-quenched Re(phen), evaluation of the PL decays of Cy5 (**Figure 5B**) could possibly reveal more accurate FRET efficiencies. The Cy5 PL decays were also fit with a 3-exponential function and the long decay time of Re(phen) (τ_{D0} = 4.51 µs) was again fixed to account for the contribution of non-quenched Re(phen), despite the fact that it was much weaker in the Cy5 PL detection channel. Therefore, the correction factor values (z_A – Equation 16 in the ESI) were also much lower. Similar to the donor emission analysis, two FRET decay times (τ_{AD1} and τ_{AD2}), their relative amplitudes (α_{AD1} and α_{AD2}), a relative donor amplitude (α_{AD0}), the donor correction factor (z_A), an average FRET decay time ($<\tau_{AD}>$), an average FRET efficiency ($<E_{FRET}>$), an average decay time of the complete decay ($<\tau>$), and a system-averaged FRET efficiency ($<E^*_{FRET}>$) could be determined (**Table 4**) by fitting and using Equation 8 and 14 to 18 (ESI).

The results clearly show that even for very low Cy5 fractions (0.1 and 0.5 wt%), the FRET efficiencies were very high (>90%), which confirmed that the intensity and lifetime evaluations of the Re(phen) donor emission strongly underestimated the FRET efficiencies and that the Re(phen) donor emission at low Cy5 fractions contained a strong contribution from non-quenched Re(phen). The FRET efficiencies constantly increased from 0.91 (for 0.1% Cy5) to 0.97 (for 5% Cy5), suggesting that for

increasing Cy5 fractions not only more FRET pairs were formed but also the average donor-acceptor distance decreased. Considering the Re(phen)-Cy5 FRET pair Förster radius of R_0= 3.7 nm (see ESI for calculation) and the measured FRET efficiencies, the average donor-acceptor distance decreased from 2.5 to 2.1 nm. These values were not accessible by simply considering the NP sizes and Re(phen) and Cy5 loading ratios. However, those volume-concentration considerations are still useful for evaluating the FRET distance calculations. When going from 0.1 to 5 wt% Cy5 loading, the average distance between Cy5 dyes in the NPs decreases from more than 12 nm to 3.5 nm, which means that at 5 wt% loading on average all Re(phen) complexes lie within a distance of less than 1.8 nm to a Cy5 dye. However, in the case of 0.1 wt% the majority of Re(phen) complexes are at distances >R_0. Whereas the average FRET distance estimations are within a reasonable range when considering the size and loading ratios of the Re(phen)-Cy5 polymer NPs, they still seem to be slightly overestimated. Considering that the very short PL decay component of Cy5 (**Figure 5B**) could not be properly resolved on the 14 µs time scale that was necessary to appropriately fit the Re(phen) donor decays, we also recorded Cy5 PL decays in a 200 ns window after pulsed excitation (**Figure 5C**). These fit results (Equation 19 to 21 in the ESI) revealed very short decay time components (amplitude-averaged lifetimes between 12.7 ns and 27.5 ns) that correspond to FRET efficiencies of ~100% and further confirmed that the formed Re(phen)-Cy5 donor-acceptor pairs provided very high FRET efficiencies, *i.e.*, all Cy5 dyes were in very close contact to at least one Re(phen) donor.

It should be noted that we cannot absolutely confirm that energy transfer occurred through FRET in these systems. However, several observations point clearly towards FRET as mechanism: First, in the steady-state measurements, clear donor quenching and acceptor sensitization were observed. Second, the lifetime analysis showed the decrease in donor fluorescence lifetime associated with FRET. Moreover, FRET efficiencies were calculated using both steady-state and time-resolved measurements, including long and short-window analysis as well as taking into account the contribution of unquenched donor. The calculated FRET efficiencies showed an increase as more acceptor was added. Other mechanisms like electron exchange and re-absorption would not exhibit the same behavior. In particular, there would be no photoluminescence lifetime changes. Also, electron transfer can only occur at very close distances (orbital overlap), whereas reabsorption would mainly occur at longer distances. The distance dependence (tuned by different percentages of acceptors) of the energy transfer efficiency is a strong evidence for FRET. Together these arguments point strongly in favor of FRET as the major mechanism of energy transfer in the studied systems.

*Table 4: Fit (from Cy5 PL decay curves in **Figure 5B**) lifetimes (τ) and amplitude fractions (α) and calculated correction factors (z_A), amplitude averaged FRET lifetimes ($<\tau_{AD}>$), average FRET efficiencies ($<E_{FRET}>$), overall amplitude-averaged lifetimes ($<\tau>$), lifetime system-averaged FRET efficiencies ($<E^*_{FRET}>$), and intensity system-averaged FRET efficiencies (int.$<E^*_{FRET}>$).*

Cy5	τ_{AD1} (µs)	α_{AD1}	τ_{AD2} (µs)	α_{AD2}	α_{AD0}	rel. errors
0.1%	0.031	0.16	0.41	0.84	0.128	5%
0.5%	0.025	0.21	0.35	0.79	0.036	5%
1.0%	0.021	0.22	0.31	0.78	0.020	5%
2.0%	0.020	0.27	0.25	0.73	0.012	5%
5.0%	0.014	0.37	0.14	0.63	0.006	5%

Cy5	z_A	$\langle\tau_{AD}\rangle$ (µs)	$\langle E_{FRET}\rangle$	$\langle\tau\rangle$ (µs)	$\langle E^*_{FRET}\rangle$	int. $\langle E^*_{FRET}\rangle$
0.1%	0.0466±15%	0.309±0.046	0.91±0.19	0.691±10%	0.81±0.13	0.08±0.02
0.5%	0.013±15%	0.268±0.031	0.93±0.16	0.248±10%	0.93±0.15	0.41±0.08
1.0%	0.0071±15%	0.244±0.026	0.93±0.16	0.161±10%	0.96±0.15	0.60±0.12
2.0%	0.0042±15%	0.183±0.020	0.95±0.16	0.110±10%	0.97±0.16	0.80±0.16
5.0%	0.0021±15%	0.093±0.010	0.97±0.16	0.059±10%	0.98±0.16	0.92±0.18

Relative errors provided in the table are related to τ and α and were estimated. Errors for z_A, $\langle\tau_{AD}\rangle$, $\langle E_{FRET}\rangle$, $\langle\tau\rangle$, $\langle E^*_{FRET}\rangle$, and int.$\langle E^*_{FRET}\rangle$ (intensity calculated system-averaged FRET efficiency with intensity errors estimated as 10%) were calculated using error propagation.

The very efficient FRET and very close donor-acceptor distances revealed by time-resolved spectroscopy are very interesting, as they allow to efficiently shift the PL of these NPs into the NIR through simple coencapsulation of the Re(phen) complexes and Cy5, without the need to chemically link the two. This results in luminescent NPs with a very large Stokes shift and a very high particle brightness through the high loading with Re(phen) complexes and a nearly complete absence of ACQ. Yet, the intuitively very positive result of high FRET efficiencies also comes with a drawback: The microsecond PL lifetimes of Re would have been very beneficial for time-gated FRET detection,[71] providing higher photon flux compared to lanthanide-based time gating (because a microsecond decay allows for 1000 times more excitations per time than millisecond decays) while still efficiently suppressing autofluorescence background (in the nano- to micro-second range). However, with a FRET efficiency close to unity, the interesting capability of shifting the emission to the NIR region (Cy5) cannot work for microsecond time-gating because the FRET-sensitized Cy5 PL decay is too fast.

To confirm the inadaptability to conventional microsecond time-gating, we used the NPs co-encapsulating Re(phen) and Cy5 for both time-gated PL detection on a conventional benchtop fluorescence plate reader and time-gated imaging inside live cells. Using pulsed excitation at 303 nm

and the shortest possible integration time of 20 µs (gate time) on a SPARK (Tecan) reader, we shifted the detection windows for both Re and Cy5 emission intensity maxima from 0 to 20 µs (delay time). After 10 µs of delay, the afterglow of the microsecond flash lamp started to decay until almost background emission was reached at a delay of 20 µs (**Figure S34**). The decay of the PL signal of the Re(phen) loaded NPs was slightly longer, whereas increasing fractions of Cy5 resulted in a progressive decrease of the additional delay toward the pure decay of the lamp afterglow. The progressive decrease of the signal delay reflected the FRET-quenched PL lifetime and intensity found during the spectroscopic characterization (*vide supra*). For the Cy5 detection channel, all signals were very similar, which confirmed the much faster PL decay of the FRET-sensitized Cy5 inside the NPs. These results were confirmed on a microsecond time-gated microscope, for which the Cy5 emission channel could not measure any Cy5 PL (data not shown because the signal only consisted of background noise).

Cellular Imaging

Considering the very strong quenching-sensitization of the Re(phen)-Cy5 donor-acceptor pair and the very large spectral separation between excitation (~300 nm) and emission (680 nm, and up to 800 nm), the large gap between Re(phen) and Cy5 emission could potentially be exploited for ratiometric sensing with significantly lower autofluorescence from the Cy5 NIR PL. Thus, we sought to evaluate the live cell imaging performance of the NPs coencapsulating Re(phen) and Cy5 with conventional steady-state fluorescence microscopy. We incubated HeLa cells for 3 h with the Re(phen)-Cy5 NPs at different loading ratios (1 wt% and 5 wt% Cy5) and then performed live cell fluorescence imaging at 520±14 nm (Re(phen) emission) and 707±8 nm (Cy5 emission) under 320 nm excitation. Taking into account that for Re(phen)-Cy5 NPs in solution the Re(phen) emission was strongly quenched and Cy5 emission strongly sensitized (**Figure 4B**), we selected a spectral bandpass filter for Re(phen) (~28 nm bandwidth) approximately twice as large as the one for Cy5 (~16 nm bandwidth).

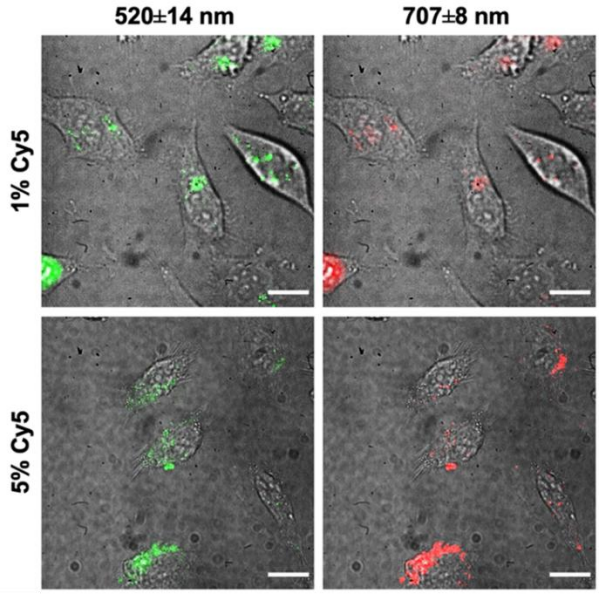

*Figure 6: Cellular Imaging of PEMA-COOH 1% NPs loaded with 40 wt% Re(phen) and 1 or 5 wt% Cy5 incubated for 3 h at 10 µg/ml, excitation (λ_{exc}) at 320±20 nm and emission (λ_{em}) at 520±14nm (green) for the donor channel and 707±8nm (red) for the acceptor channel. The images show the overlay of DIC and fluorescence, Re(phen) PL intensity is colored in green, Cy5 PL intensity is colored in red. The first-row show images of NPs loaded with **40 wt% [Re(phen)] and 1 wt% Cy5** and the second-row show images of **NPs loaded with 40 wt% [Re(phen)]** and **5 wt% Cy5**. Images of the NPs were acquired using an Olympus IX83 microscope with EMCCD camera (Andor) with an acquisition time of 500ms, x500 EM gain and illuminated with continuous wave illumination source at a power of 82W. Scale bars are 20 µm in length in all images.*

For both Cy5 fractions (1 wt% and 5 wt%), clear PL signals of both Re(phen) and Cy5 could be detected inside the HeLa cells (**Figure 6**) with intensities that were adequate for ratiometric detection. The relative Cy5-to-Re(phen) PL intensities clearly increased with increasing Cy5 fraction (**Figure S35**), which confirmed the FRET behavior found for NPs in solution (cf. **Figure 4B**). Control experiments showed that there was no significant Cy5 emission detectable when Re(phen) loaded NPs (without Cy5) were incubated with HeLa cells (**Figure S36)** and only autofluorescence (in the Re(phen) detection channel) and very faint Cy5 fluorescence (in the Cy5 detection channel) were detectable when Cy5 loaded NPs (without Re(phen)) were incubated with HeLa cells (**Figure S37)**. Imaging from top to bottom (z-stacking) through the Hela cells incubated with NPs confirmed their good internalization inside the cell (**Figure S38**). This was in good agreement with results obtained previously on similar NPs.[29,52] We suppose that the formation of a protein corona in the presence of serum[22] facilitates efficient internalization of these NPs. The morphology of all imaged cells was unaffected, which showed that the endocytosis of the NPs had no significant impact on the live cells.

Conclusion

In this work, we demonstrate encapsulation of very high amounts of luminescent transition-metal complexes in polymer NPs made of polymethacrylates and biodegradable polyesters and analyzed the physicochemical and photophysical properties of the resulting materials in detail. Variation of the polymers used allowed tuning of particle size, from 20 to 70 nm, encapsulating up to 40 wt% of Re

complexes corresponding to close to 10,000 Re complexes per NP. The PL QYs of the Re complexes increased strongly upon encapsulation in polymer NPs, reaching close to 50% in some cases, which resulted in probes with PL brightness of up to 10^8 M^{-1} cm^{-1} and lifetimes of the order of 3-4 µs. Encapsulation thus helped to create very bright luminescent probes for use in bioimaging based on luminescent Re complexes. However, in view of excitation in the UV and emission around 500 nm, a strong autofluorescence background was expected in bioimaging applications. We could show that this can be overcome by co-encapsulation of the NIR dye Cy5 in the Re complex loaded NPs, which resulted in a shift of the emission into the NIR due to energy transfer. A deeper analysis of the photophysics of the system allowed to unravel the underlying mechanisms. Indeed, lifetime measurements showed very efficient FRET from the Re complex donors to the Cy5 acceptors and revealed a very close proximity of the encapsulated luminophores. This resulted in very bright, visible and NIR emitting NPs, which could be used for cellular imaging and showed good internalization and high contrast in the two wavelength regions, and showed a very large separation of excitation and emission wavelengths. Thus, simple co-encapsulation of different luminescent compounds, proved to be a powerful strategy to tailor and optimize the emission properties of nanoprobes - without requiring a covalent link - even for such differing entities as organic fluorophores and transition metal compounds, opening the way to new classes of luminescent probes. Though the very efficient FRET made microsecond time-gated imaging in the NIR impossible, the resulting objects showed a high brightness for emission in the NIR in combination with lifetimes in the range of hundreds of nanoseconds, in this way combining advantages of the two types of emitters. In this way, by relying on set-ups allowing very fast TG, sub-µs TG imaging may become possible, combining higher photon flux than what is typically obtained in La and transition metal-based millisecond and microsecond TG with efficient background removal. Our analysis of the photophysics of the obtained materials also showed that careful analysis of materials properties leads to a deepened understanding of such complex systems, which is the key to discover new types of materials with new properties enabling new applications.

Acknowledgements

The authors thank the French National Research Agency, ANR (LAPIN project n° ANR-20-CE09-0021-02). Financial support is gratefully acknowledged (LJC and RCK) from the French Ministère de l'Education Nationale et de la Recherche, Frontier Research in Chemistry Foundation (LabEx CSC, ANR-10-LABX-0026_CSC), and the French National Research Agency, ANR (LUCAS project n°ANR-19-CE29-0014-01). AC and AR thank the Frontier Research in Chemistry Foundation, Fondation Jean-Marie Lehn, Emerging Investigators Grant. NF, TG, and NH thank Labex SynOrg (ANR-11-LABX-0029),

University of Rouen Normandy, Normandy University, INSA Rouen Normandy, the Centre National de la Recherche Scientifique (CNRS), European Regional Development Fund (ERDF), Carnot Insitute I2C, XL-Chem graduate school (ANR-18-EURE-0020 XL CHEM), and Region Normandie, for financial support. NH thanks the Brain Pool program funded by the Ministry of Science and ICT through the National Research Foundation of Korea (2021H1D3A2A02049589) and Seoul National University. RCK also thanks the Royal Society of Chemistry Research Fund Grant (RF19-0248). The authors also acknowledge the support and the use of resources of the French Infrastructure for Integrated Structural Biology FRISBI ANR-10-INBS-05 and of Instruct-ERIC and especially C. Crucifix for help with electron microscopy.

Conflicts of interest

The authors declare no conflicts of interest.

References

(1) Han, X.; Xu, K.; Taratula, O.; Farsad, K. Applications of Nanoparticles in Biomedical Imaging. *Nanoscale* **2019**, *11* (3), 799–819. https://doi.org/10.1039/C8NR07769J.

(2) Lauwerends, L. J.; van Driel, P. B. A. A.; Baatenburg de Jong, R. J.; Hardillo, J. A. U.; Koljenovic, S.; Puppels, G.; Mezzanotte, L.; Löwik, C. W. G. M.; Rosenthal, E. L.; Vahrmeijer, A. L.; Keereweer, S. Real-Time Fluorescence Imaging in Intraoperative Decision Making for Cancer Surgery. *Lancet Oncol.* **2021**, *22* (5), e186–e195. https://doi.org/10.1016/S1470-2045(20)30600-8.

(3) Elf, J.; Barkefors, I. Single-Molecule Kinetics in Living Cells. *Annu. Rev. Biochem.* **2019**, *88*, 635–659. https://doi.org/10.1146/annurev-biochem-013118-110801.

(4) Zhang, K. Y.; Yu, Q.; Wei, H.; Liu, S.; Zhao, Q.; Huang, W. Long-Lived Emissive Probes for Time-Resolved Photoluminescence Bioimaging and Biosensing. *Chem. Rev.* **2018**, *118* (4), 1770–1839. https://doi.org/10.1021/acs.chemrev.7b00425.

(5) Gill, M. R.; Garcia-Lara, J.; Foster, S. J.; Smythe, C.; Battaglia, G.; Thomas, J. A. A Ruthenium(II) Polypyridyl Complex for Direct Imaging of DNA Structure in Living Cells. *Nat. Chem.* **2009**, *1* (8), 662–667. https://doi.org/10.1038/nchem.406.

(6) Dröge, F.; Noakes, F. F.; Archer, S. A.; Sreedharan, S.; Raza, A.; Robertson, C. C.; MacNeil, S.; Haycock, J. W.; Carson, H.; Meijer, A. J. H. M.; Smythe, C. G. W.; Bernardino de la Serna, J.; Dietzek-Ivanšić, B.; Thomas, J. A. A Dinuclear Osmium(II) Complex Near-Infrared Nanoscopy Probe for Nuclear DNA. *J. Am. Chem. Soc.* **2021**, *143* (48), 20442–20453. https://doi.org/10.1021/jacs.1c10325.

(7) Day, A. H.; Übler, M. H.; Best, H. L.; Lloyd-Evans, E.; Mart, R. J.; Fallis, I. A.; Allemann, R. K.; Al-Wattar, E. A. H.; Keymer, N. I.; Buurma, N. J.; Pope, S. J. A. Targeted Cell Imaging Properties of a Deep Red Luminescent Iridium(III) Complex Conjugated with a c-Myc Signal Peptide. *Chem. Sci.* **2020**, *11* (6), 1599–1606. https://doi.org/10.1039/C9SC05568A.

(8) Holden, L.; Burke, C. S.; Cullinane, D.; Keyes, T. E. Strategies to Promote Permeation and Vectorization, and Reduce Cytotoxicity of Metal Complex Luminophores for Bioimaging and Intracellular Sensing. *RSC Chem. Biol.* **2021**, *2* (4), 1021–1049. https://doi.org/10.1039/D1CB00049G.

(9) Amoroso, A. J.; Coogan, M. P.; Dunne, J. E.; Fernández-Moreira, V.; Hess, J. B.; Hayes, A. J.; Lloyd, D.; Millet, C.; Pope, S. J. A.; Williams, C. Rhenium Fac Tricarbonyl Bisimine Complexes: Biologically Useful Fluorochromes for Cell Imaging Applications. *Chem. Commun.* **2007**, No. 29, 3066–3068. https://doi.org/10.1039/B706657K.

(10) Lo, K. K.-W.; Zhang, K. Y.; Li, S. P.-Y. Recent Exploitation of Luminescent Rhenium(I) Tricarbonyl Polypyridine Complexes as Biomolecular and Cellular Probes. *Eur. J. Inorg. Chem.* **2011**, *2011* (24), 3551–3568. https://doi.org/10.1002/ejic.201100469.

(11) Lo, K. K.-W.; Choi, A. W.-T.; Law, W. H.-T. Applications of Luminescent Inorganic and Organometallic Transition Metal Complexes as Biomolecular and Cellular Probes. *Dalton Trans.* **2012**, *41* (20), 6021–6047. https://doi.org/10.1039/C2DT11892K.

(12) Hostachy, S.; Policar, C.; Delsuc, N. Re(I) Carbonyl Complexes: Multimodal Platforms for Inorganic Chemical Biology. *Coord. Chem. Rev.* **2017**, *351*, 172–188. https://doi.org/10.1016/j.ccr.2017.05.004.

(13) Lee, L. C.-C.; Lo, K. K.-W. Strategic Design of Luminescent Rhenium(I), Ruthenium(II), and Iridium(III) Complexes as Activity-Based Probes for Bioimaging and Biosensing. *Chem. – Asian J.* **2022**, *17* (22), e202200840. https://doi.org/10.1002/asia.202200840.

(14) Rampazzo, E.; Genovese, D.; Palomba, F.; Prodi, L.; Zaccheroni, N. NIR-Fluorescent Dye Doped Silica Nanoparticles for in Vivo Imaging, Sensing and Theranostic. *Methods Appl. Fluoresc.* **2018**, *6* (2), 022002. https://doi.org/10.1088/2050-6120/aa8f57.

(15) Yang, S.; Li, Y. Fluorescent Hybrid Silica Nanoparticles and Their Biomedical Applications. *WIREs Nanomedicine Nanobiotechnology* **2020**, *12* (3), e1603. https://doi.org/10.1002/wnan.1603.

(16) Li, K.; Liu, B. Polymer-Encapsulated Organic Nanoparticles for Fluorescence and Photoacoustic Imaging. *Chem. Soc. Rev.* **2014**, *43* (18), 6570–6597. https://doi.org/10.1039/C4CS00014E.

(17) Reisch, A.; Klymchenko, A. S. Fluorescent Polymer Nanoparticles Based on Dyes: Seeking Brighter Tools for Bioimaging. *Small* **2016**, *12* (15), 1968–1992. https://doi.org/10.1002/smll.201503396.

(18) Visaveliya, N. R.; Köhler, J. M. Softness Meets with Brightness: Dye-Doped Multifunctional Fluorescent Polymer Particles via Microfluidics for Labeling. *Adv. Opt. Mater.* **2021**, *9* (13), 2002219. https://doi.org/10.1002/adom.202002219.

(19) Ashoka, A. H.; Aparin, I. O.; Reisch, A.; Klymchenko, A. S. Brightness of Fluorescent Organic Nanomaterials. *Chem. Soc. Rev.* **2023**. https://doi.org/10.1039/D2CS00464J.

(20) Sobska, J.; Andreiuk, B.; Aparin, I. O.; Reisch, A.; Krezel, W.; Klymchenko, A. S. Counterion-Insulated near-Infrared Dyes in Biodegradable Polymer Nanoparticles for in Vivo Imaging. *Nanoscale Adv.* **2021**, *4* (1), 39–48. https://doi.org/10.1039/d1na00649e.

(21) Andreiuk, B.; Reisch, A.; Lindecker, M.; Follain, G.; Peyriéras, N.; Goetz, J. G.; Klymchenko, A. S. Fluorescent Polymer Nanoparticles for Cell Barcoding In Vitro and In Vivo. *Small* **2017**, *13* (38), 1701582. https://doi.org/10.1002/smll.201701582.

(22) Runser, A.; Dujardin, D.; Ernst, P.; Klymchenko, A. S.; Reisch, A. Zwitterionic Stealth Dye-Loaded Polymer Nanoparticles for Intracellular Imaging. *ACS Appl. Mater. Interfaces* **2020**, *12* (1), 117–125. https://doi.org/10.1021/acsami.9b15396.

(23) Egloff, S.; Melnychuk, N.; Cruz Da Silva, E.; Reisch, A.; Martin, S.; Klymchenko, A. S. Amplified Fluorescence in Situ Hybridization by Small and Bright Dye-Loaded Polymeric Nanoparticles. *ACS Nano* **2022**, *16* (1), 1381–1394. https://doi.org/10.1021/acsnano.1c09409.

(24) Melnychuk, N.; Egloff, S.; Runser, A.; Reisch, A.; Klymchenko, A. S. Light-Harvesting Nanoparticle Probes for FRET-Based Detection of Oligonucleotides with Single-Molecule Sensitivity. *Angew. Chem. Int. Ed.* **2020**, *59* (17), 6811–6818. https://doi.org/10.1002/anie.201913804.

(25) Egloff, S.; Melnychuk, N.; Reisch, A.; Martin, S.; Klymchenko, A. S. Enzyme-Free Amplified Detection of Cellular MicroRNA by Light-Harvesting Fluorescent Nanoparticle Probes. *Biosens. Bioelectron.* **2021**, *179*, 113084. https://doi.org/10.1016/j.bios.2021.113084.

(26) Cardoso Dos Santos, M.; Runser, A.; Bartenlian, H.; Nonat, A. M.; Charbonnière, L. J.; Klymchenko, A. S.; Hildebrandt, N.; Reisch, A. Lanthanide-Complex-Loaded Polymer Nanoparticles for Background-Free Single-Particle and Live-Cell Imaging. *Chem. Mater.* **2019**, *31* (11), 4034–4041. https://doi.org/10.1021/acs.chemmater.9b00576.

(27) Severi, C.; Lahtinen, S.; Rosenberg, J.; Reisch, A.; Soukka, T.; Klymchenko, A. S. Lanthanide-Based Bulky Counterions against Aggregation-Caused Quenching of Dyes in Fluorescent Polymeric Nanoparticles. *Aggregate* **2022**, *3* (1), e130. https://doi.org/10.1002/agt2.130.

(28) Haye, L.; Diriwari, P. I.; Alhalabi, A.; Gallavardin, T.; Combes, A.; Klymchenko, A. S.; Hildebrandt, N.; Le Guével, X.; Reisch, A. Enhancing Near Infrared II Emission of Gold Nanoclusters via Encapsulation in Small Polymer Nanoparticles. *Adv. Opt. Mater. n/a* (n/a), 2201474. https://doi.org/10.1002/adom.202201474.

(29) Reisch, A.; Didier, P.; Richert, L.; Oncul, S.; Arntz, Y.; Mély, Y.; Klymchenko, A. S. Collective Fluorescence Switching of Counterion-Assembled Dyes in Polymer Nanoparticles. *Nat. Commun.* **2014**, *5*, 4089. https://doi.org/10.1038/ncomms5089.

(30) Trofymchuk, K.; Reisch, A.; Didier, P.; Fras, F.; Gilliot, P.; Mely, Y.; Klymchenko, A. S. Giant Light-Harvesting Nanoantenna for Single-Molecule Detection in Ambient Light. *Nat. Photonics* **2017**, *11* (10), 657. https://doi.org/10.1038/s41566-017-0001-7.

(31) Li, B.; Kwok, K. M.; Zeng, H. C. Versatile Hollow ZSM-5 Nanoreactors Loaded with Tailorable Metal Catalysts for Selective Hydrogenation Reactions. *ACS Appl. Mater. Interfaces* **2021**, *13* (17), 20524–20538. https://doi.org/10.1021/acsami.1c01916.

(32) Salavati-Niasari, M.; Shakouri-Arani, M.; Davar, F. Flexible Ligand Synthesis, Characterization and Catalytic Oxidation of Cyclohexane with Host (Nanocavity of Zeolite-Y)/Guest (Mn(II), Co(II), Ni(II) and Cu(II) Complexes of Tetrahydro-Salophen) Nanocomposite Materials. *Microporous Mesoporous Mater.* **2008**, *116* (1), 77–85. https://doi.org/10.1016/j.micromeso.2008.03.015.

(33) Shilpa, E. R.; Gayathri, V. Encapsulation of Cu(II)[2-(2′-Hydroxyphenyl)Benzimidazole]2 within Zeolite Nano-Cavity: Structural Properties and Its Catalytic Activity towards Phenol and Styrene Oxidation. *J. Environ. Chem. Eng.* **2016**, *4* (4, Part A), 4194–4206. https://doi.org/10.1016/j.jece.2016.09.022.

(34) Xu, L.; Zhang, J.; Li, Z.; Ma, Q.; Wang, Y.; Cui, F.; Cui, T. In Situ Generation of Ultrasmall Sized and Highly Dispersed CuO Nanoparticles Embedded in Silica Matrix and Their Catalytic Application. *New J. Chem.* **2018**, *43* (1), 520–526. https://doi.org/10.1039/C8NJ04517H.

(35) Zhang, P.; Huang, H.; Huang, J.; Chen, H.; Wang, J.; Qiu, K.; Zhao, D.; Ji, L.; Chao, H. Noncovalent Ruthenium(II) Complexes–Single-Walled Carbon Nanotube Composites for Bimodal Photothermal and Photodynamic Therapy with Near-Infrared Irradiation. *ACS Appl. Mater. Interfaces* **2015**, *7* (41), 23278–23290. https://doi.org/10.1021/acsami.5b07510.

(36) Shen, J.; Kim, H.-C.; Wolfram, J.; Mu, C.; Zhang, W.; Liu, H.; Xie, Y.; Mai, J.; Zhang, H.; Li, Z.; Guevara, M.; Mao, Z.-W.; Shen, H. A Liposome Encapsulated Ruthenium Polypyridine Complex as a Theranostic Platform for Triple-Negative Breast Cancer. *Nano Lett.* **2017**, *17* (5), 2913–2920. https://doi.org/10.1021/acs.nanolett.7b00132.

(37) Lu, M.; Chen, F.; Noy, J.-M.; Lu, H.; Stenzel, M. H. Enhanced Antimetastatic Activity of the Ruthenium Anticancer Drug RAPTA-C Delivered in Fructose-Coated Micelles. *Macromol. Biosci.* **2017**, *17* (10), 1600513. https://doi.org/10.1002/mabi.201600513.

(38) Bœuf, G.; Roullin, G. V.; Moreau, J.; Van Gulick, L.; Zambrano Pineda, N.; Terryn, C.; Ploton, D.; Andry, M. C.; Chuburu, F.; Dukic, S.; Molinari, M.; Lemercier, G. Encapsulated Ruthenium(II) Complexes in Biocompatible Poly(d,l-Lactide-Co-Glycolide) Nanoparticles for Application in

Photodynamic Therapy. *ChemPlusChem* **2014**, *79* (1), 171–180. https://doi.org/10.1002/cplu.201300242.

(39) Villemin, E.; Ong, Y. C.; Thomas, C. M.; Gasser, G. Polymer Encapsulation of Ruthenium Complexes for Biological and Medicinal Applications. *Nat. Rev. Chem.* **2019**, *3* (4), 261–282. https://doi.org/10.1038/s41570-019-0088-0.

(40) António, J. P. M.; Gandioso, A.; Nemati, F.; Soliman, N.; Vinck, R.; Sun, F.; Robert, C.; Burckel, P.; Decaudin, D.; Thomas, C. M.; Gasser, G. Polymeric Encapsulation of a Ruthenium(II) Polypyridyl Complex: From Synthesis to in Vivo Studies against High-Grade Epithelial Ovarian Cancer. *Chem. Sci.* **2023**, *14* (2), 362–371. https://doi.org/10.1039/D2SC05693C.

(41) Aubert, T.; Ledneva, A. Y.; Grasset, F.; Kimoto, K.; Naumov, N. G.; Molard, Y.; Saito, N.; Haneda, H.; Cordier, S. Synthesis and Characterization of A4[Re6Q8L6]@SiO2 Red-Emitting Silica Nanoparticles Based on Re6 Metal Atom Clusters (A = Cs or K, Q = S or Se, and L = OH or CN). *Langmuir* **2010**, *26* (23), 18512–18518. https://doi.org/10.1021/la103784v.

(42) Li, X.; Zhang, Y.; Chen, H.; Sun, J.; Feng, F. Protein Nanocages for Delivery and Release of Luminescent Ruthenium(II) Polypyridyl Complexes. *ACS Appl. Mater. Interfaces* **2016**, *8* (35), 22756–22761. https://doi.org/10.1021/acsami.6b07038.

(43) Caspar, J. V.; Meyer, T. J. Application of the Energy Gap Law to Nonradiative, Excited-State Decay. *J. Phys. Chem.* **1983**, *87* (6), 952–957. https://doi.org/10.1021/j100229a010.

(44) Hong, G.; Antaris, A. L.; Dai, H. Near-Infrared Fluorophores for Biomedical Imaging. *Nat. Biomed. Eng.* **2017**, *1* (1), 0010. https://doi.org/10.1038/s41551-016-0010.

(45) Rosiuk, V.; Runser, A.; Klymchenko, A.; Reisch, A. Controlling Size and Fluorescence of Dye-Loaded Polymer Nanoparticles through Polymer Design. *Langmuir* **2019**, *35* (21), 7009–7017. https://doi.org/10.1021/acs.langmuir.9b00721.

(46) Wrighton, M.; Morse, D. L. Nature of the Lowest Excited State in Tricarbonylchloro-1,10-Phenanthrolinerhenium(I) and Related Complexes. *J. Am. Chem. Soc.* **1974**, *96* (4), 998–1003. https://doi.org/10.1021/ja00811a008.

(47) Knighton, R. C.; Soro, L. K.; Thor, W.; Strub, J.-M.; Cianférani, S.; Mély, Y.; Lenertz, M.; Wong, K.-L.; Platas-Iglesias, C.; Przybilla, F.; Charbonnière, L. J. Upconversion in a d–f [RuYb3] Supramolecular Assembly. *J. Am. Chem. Soc.* **2022**, *144* (29), 13356–13365. https://doi.org/10.1021/jacs.2c05037.

(48) Yue, Y.; Grusenmeyer, T.; Ma, Z.; Zhang, P.; Pham, T. T.; Mague, J. T.; Donahue, J. P.; Schmehl, R. H.; Beratan, D. N.; Rubtsov, I. V. Evaluating the Extent of Intramolecular Charge Transfer in the Excited States of Rhenium(I) Donor-Acceptor Complexes with Time-Resolved Vibrational Spectroscopy. *J. Phys. Chem. B* **2013**, *117* (49), 15903–15916. https://doi.org/10.1021/jp409628e.

(49) Aparin, I. O.; Adarsh, N.; Reisch, A.; Klymchenko, A. S. Bulky Hydrophobic Counterions for Suppressing Aggregation-Caused Quenching of Ionic Dyes in Fluorescent Nanoparticles. In *Handbook of Aggregation-Induced Emission*; John Wiley & Sons, Ltd, 2022; pp 511–540. https://doi.org/10.1002/9781119643098.ch59.

(50) Andreiuk, B.; Reisch, A.; Bernhardt, E.; Klymchenko, A. S. Fighting Aggregation-Caused Quenching and Leakage of Dyes in Fluorescent Polymer Nanoparticles: Universal Role of Counterion. *Chem. – Asian J.* **2019**, *14* (6), 836–846. https://doi.org/10.1002/asia.201801592.

(51) Krossing, I.; Raabe, I. Noncoordinating Anions—Fact or Fiction? A Survey of Likely Candidates. *Angew. Chem. Int. Ed.* **2004**, *43* (16), 2066–2090. https://doi.org/10.1002/anie.200300620.

(52) Andreiuk, B.; Reisch, A.; Lindecker, M.; Follain, G.; Peyriéras, N.; Goetz, J. G.; Klymchenko, A. S. Fluorescent Polymer Nanoparticles for Cell Barcoding In Vitro and In Vivo. *Small* **2017**, *13* (38), 1701582. https://doi.org/10.1002/smll.201701582.

(53) Peng, X.; Yang, Z.; Wang, J.; Fan, J.; He, Y.; Song, F.; Wang, B.; Sun, S.; Qu, J.; Qi, J.; Yan, M. Fluorescence Ratiometry and Fluorescence Lifetime Imaging: Using a Single Molecular Sensor for Dual Mode Imaging of Cellular Viscosity. *J. Am. Chem. Soc.* **2011**, *133* (17), 6626–6635. https://doi.org/10.1021/ja1104014.

(54) Chakraborty, I.; Jimenez, J.; Sameera, W. M. C.; Kato, M.; Mascharak, P. K. Luminescent Re(I) Carbonyl Complexes as Trackable PhotoCORMs for CO Delivery to Cellular Targets. *Inorg. Chem.* **2017**, *56* (5), 2863–2873. https://doi.org/10.1021/acs.inorgchem.6b02999.

(55) Sun, S.-S.; Zavalij, P. Y.; Lees, A. J. Aceto-nitrile-tri-carbonyl-(2,9-Di-methyl-4,7-Di-phenyl-1,10-Phenanthroline)-rhenium(I) Hexa-fluoro-phosphate. *Acta Crystallogr. Sect. E Struct. Rep. Online* **2001**, *57* (3), m119–m121. https://doi.org/10.1107/S1600536801003440.

(56) Ishida, H.; Tobita, S.; Hasegawa, Y.; Katoh, R.; Nozaki, K. Recent Advances in Instrumentation for Absolute Emission Quantum Yield Measurements. *Coord. Chem. Rev.* **2010**, *254* (21–22), 2449–2458. https://doi.org/10.1016/j.ccr.2010.04.006.

(57) Lepeltier, E.; Bourgaux, C.; Couvreur, P. Nanoprecipitation and the “Ouzo Effect”: Application to Drug Delivery Devices. *Adv. Drug Deliv. Rev.* **2014**, *71*, 86–97. https://doi.org/10.1016/j.addr.2013.12.009.

(58) Chen, T.; Peng, Y.; Qiu, M.; Yi, C.; Xu, Z. Recent Advances in Mixing-Induced Nanoprecipitation: From Creating Complex Nanostructures to Emerging Applications beyond Biomedicine. *Nanoscale* **2023**. https://doi.org/10.1039/D3NR00280B.

(59) Kneas, K. A.; Xu, W.; Demas, J. N.; DeGraff, B. A.; Zipp, A. P. Luminescence-Based Oxygen Sensors: ReL(CO)3Cl and ReL(CO)3CN Complexes on Copolymer Supports. *J. Fluoresc.* **1998**, *8* (4), 295–300. https://doi.org/10.1023/A:1020560128916.

(60) Ramos, L. D.; Cruz, H. M. da; Frin, K. P. M. Photophysical Properties of Rhenium(I) Complexes and Photosensitized Generation of Singlet Oxygen. *Photochem. Photobiol. Sci.* **2017**, *16* (4), 459–466. https://doi.org/10.1039/C6PP00364H.

(61) Wang, C.; Kitzmann, W. R.; Weigert, F.; Förster, C.; Wang, X.; Heinze, K.; Resch-Genger, U. Matrix Effects on Photoluminescence and Oxygen Sensitivity of a Molecular Ruby. *ChemPhotoChem* **2022**, *6* (6), e202100296. https://doi.org/10.1002/cptc.202100296.

(62) Onoe, S.; Temma, T.; Shimizu, Y.; Ono, M.; Saji, H. Investigation of Cyanine Dyes for in Vivo Optical Imaging of Altered Mitochondrial Membrane Potential in Tumors. *Cancer Med.* **2014**, *3* (4), 775–786. https://doi.org/10.1002/cam4.252.

(63) Liu, J.-X.; Mei, S.-L.; Chen, X.-H.; Yao, C.-J. Recent Advances of Near-Infrared (NIR) Emissive Metal Complexes Bridged by Ligands with N- and/or O-Donor Sites. *Crystals* **2021**, *11* (2), 155. https://doi.org/10.3390/cryst11020155.

(64) Artem’ev, A. V.; Petyuk, M. Yu.; Berezin, A. S.; Gushchin, A. L.; Sokolov, M. N.; Bagryanskaya, I. Yu. Synthesis and Study of Re(I) Tricarbonyl Complexes Based on Octachloro-1,10-Phenanthroline: Towards Deep Red-to-NIR Emitters. *Polyhedron* **2021**, *209*, 115484. https://doi.org/10.1016/j.poly.2021.115484.

(65) Knighton, R. C.; Dapin, S.; Beer, P. D. Luminescent Anion Sensing by Transition-Metal Dipyridylbenzene Complexes Incorporated into Acyclic, Macrocyclic and Interlocked Hosts. *Chem. – Eur. J.* **2020**, *26* (23), 5288–5296. https://doi.org/10.1002/chem.202000661.

(66) Shakirova, J. R.; Nayeri, S.; Jamali, S.; Porsev, V. V.; Gurzhiy, V. V.; Levin, O. V.; Koshevoy, I. O.; Tunik, S. P. Targeted Synthesis of NIR Luminescent Rhenium Diimine Cis,Trans-[Re( )(CO)2(L)2]N+ Complexes Containing N-Donor Axial Ligands: Photophysical, Electrochemical, and Theoretical Studies. *ChemPlusChem* **2020**, *85* (11), 2518–2527. https://doi.org/10.1002/cplu.202000597.

(67) Zhang, W.; Liu, Y.; Gao, Q.; Liu, C.; Song, B.; Zhang, R.; Yuan, J. A Ruthenium(II) Complex–Cyanine Energy Transfer Scaffold Based Luminescence Probe for Ratiometric Detection and

Imaging of Mitochondrial Peroxynitrite. *Chem. Commun.* **2018**, *54* (97), 13698–13701. https://doi.org/10.1039/C8CC08061E.

(68) Chen, C.; Corry, B.; Huang, L.; Hildebrandt, N. FRET-Modulated Multihybrid Nanoparticles for Brightness-Equalized Single-Wavelength Barcoding. *J. Am. Chem. Soc.* **2019**, *141* (28), 11123–11141. https://doi.org/10.1021/jacs.9b03383.

(69) Hildebrandt, N. How to Apply FRET: From Experimental Design to Data Analysis. In *FRET – Förster Resonance Energy Transfer*; John Wiley & Sons, Ltd, 2013; pp 105–163. https://doi.org/10.1002/9783527656028.ch05.

(70) Wegner, K. D.; Lanh, P. T.; Jennings, T.; Oh, E.; Jain, V.; Fairclough, S. M.; Smith, J. M.; Giovanelli, E.; Lequeux, N.; Pons, T.; Hildebrandt, N. Influence of Luminescence Quantum Yield, Surface Coating, and Functionalization of Quantum Dots on the Sensitivity of Time-Resolved FRET Bioassays. *ACS Appl. Mater. Interfaces* **2013**, *5* (8), 2881–2892. https://doi.org/10.1021/am3030728.

(71) Zwier, J. M.; Hildebrandt, N. Time-Gated FRET Detection for Multiplexed Biosensing. In *Reviews in Fluorescence 2016*; Geddes, C. D., Ed.; Reviews in Fluorescence; Springer International Publishing: Cham, 2017; pp 17–43. https://doi.org/10.1007/978-3-319-48260-6_3.